# Lawrence Berkeley National Laboratory

## Title

Attosecond spectroscopy of size-resolved water clusters

## Permalink

https://escholarship.org/uc/item/5s2468ww

## Journal

Nature, 609(7927)

## ISSN

0028-0836

## Authors

Gong, Xiaochun

Heck, Saijoscha

Jelovina, Denis

et al.

## Publication Date

2022-09-15

## DOI

10.1038/s41586-022-05039-8

## Copyright Information

Peer reviewed

# Attosecond spectroscopy of size-resolved water clusters

X. Gong[1,2,*], S. Heck[1,*], D. Jelovina[1], C. Perry[1], K. Zinchenko[1], R. Lucchese[3], H. J. Wörner[1,†]

[1]*Laboratorium für Physikalische Chemie, ETH Zürich, 8093 Zürich, Switzerland*

[2]*State Key Laboratory of Precision Spectroscopy, East China Normal University, Shanghai, China*

[3]*Chemical Sciences Division, Lawrence Berkeley National Laboratory, Berkeley, California 94720, USA*

∗ *These authors contributed equally to this work.*

† *e-mail: hwoerner@ethz.ch*

**Electron dynamics in water are of fundamental importance for a broad range of phenomena[1–3], but their real-time study faces numerous conceptual and methodological challenges[4–6]. Here, we introduce attosecond size-resolved cluster spectroscopy and build up a molecular-level understanding of the attosecond electron dynamics in water. We measure the effect that the addition of single water molecules has on the photoionization time delays[7–11] of water clusters. We find a continuous increase of the delay for clusters containing up to 4-5 molecules and little change towards larger clusters. We show that these delays are proportional to the spatial extension of the created electron hole, which first increases with cluster size and then partially localizes through the onset of structural disorder that is characteristic of large clusters and bulk liquid water. These results suggest a previously unknown sensitivity of photoionization delays to electron-hole delocalization and indicate a direct link between electronic structure and attosecond photoionization dynamics. Our results offer novel perspectives for studying electron/hole delocalization and its attosecond dynamics.**

Electronic dynamics in water play a central role in a broad range of scientific and technological research areas ranging from radiation chemistry to photocatalysis. The dynamics induced by ionization of water are of particular relevance since they initiate the processes underlying radiation damage[2,3,12]. The ionization of water is predicted to lead to the formation of a delocalized electron hole, followed by its localization on one water molecule and proton transfer to a neighboring molecule, forming $H_3O^+$ and $OH$[13]. The latter step has been time-resolved only very recently using one-photon extreme-ultraviolet (XUV) photoionization of water clusters[4] and strong-field ionization of liquid water[5]. Both experiments independently determined a 30-50 fs time scale for proton transfer. The formation of the delocalized electron hole, as well as its localization have so far escaped experimental scrutiny because of their sub-femtosecond time scales. The extent to which the initial hole is delocalized, how fast it localizes and how these attosecond electron-hole dynamics predetermine the subsequent nuclear motion are fundamental unknown aspects that would greatly improve our understanding of the primary processes governing ionization-induced reaction dynamics in aqueous solutions.

In this work, we access the attosecond time scale of the photoionization dynamics of water on the molecular level by introducing attosecond size-resolved cluster spectroscopy (ASCS). Coupling attosecond interferometry[9,11,14,15] with electron-ion coincidence spectroscopy, we determine photoionization delays for water clusters of increasing size, achieving single-molecule resolution. Photoionization time delays of $(H_2O)_n$ are found to continuously increase from $n = 1$ to $n = 4-5$. We show that this increase directly reflects the augmenting delocalization of the electron hole created in the ionization process. For these small clusters, we find a linear relationship between the

photoionization time delays and the first moment of the electron-hole density created in the ionization process. Beyond $n = 4 - 5$ the photoionization delays vary little, an effect that we attribute to the partial localization of the electron hole caused by the onset of structural disorder characteristic of larger clusters and bulk liquid water. These assignments are further confirmed by calculations on the O-1s photoionization delays of water clusters, which display these effects even more clearly owing to the atomic character of the orbitals. As we show below, the present results also confirm the interpretation of photoionization delays from liquid water[6]. Finally, we show that the sensitivity of photoionization delays to electron delocalization also extends to other systems, as illustrated by calculations on polyacetylene systems.

Our work thus also reveals a possible experimental access to the spatial delocalization of electronic wave functions, which has always been difficult to characterize. Electron delocalization plays a fundamental role in the properties of solids, where the perfect translational symmetry of single crystals creates fully delocalized electronic wave functions (or Bloch waves), which are disrupted by local disorder in a phenomenon known as Anderson localization[16, 17]. The delocalization of electronic wave functions is also central for understanding the aromaticity of molecules, charge transfer between a metal atom and its ligands, or between a solute and a solvent. Evidence for the partial delocalization of electrons in water has been obtained from calculations on bulk water[18, 19] and water clusters[20], as well as from the shape of the $3a_1$ photoelectron band of liquid water[21] and its evolution in highly concentrated salt solutions[22]. However, both a quantitative measurement technique and the ability to experimentally separate the influence of electronic and structural dynamics have been missing so far.
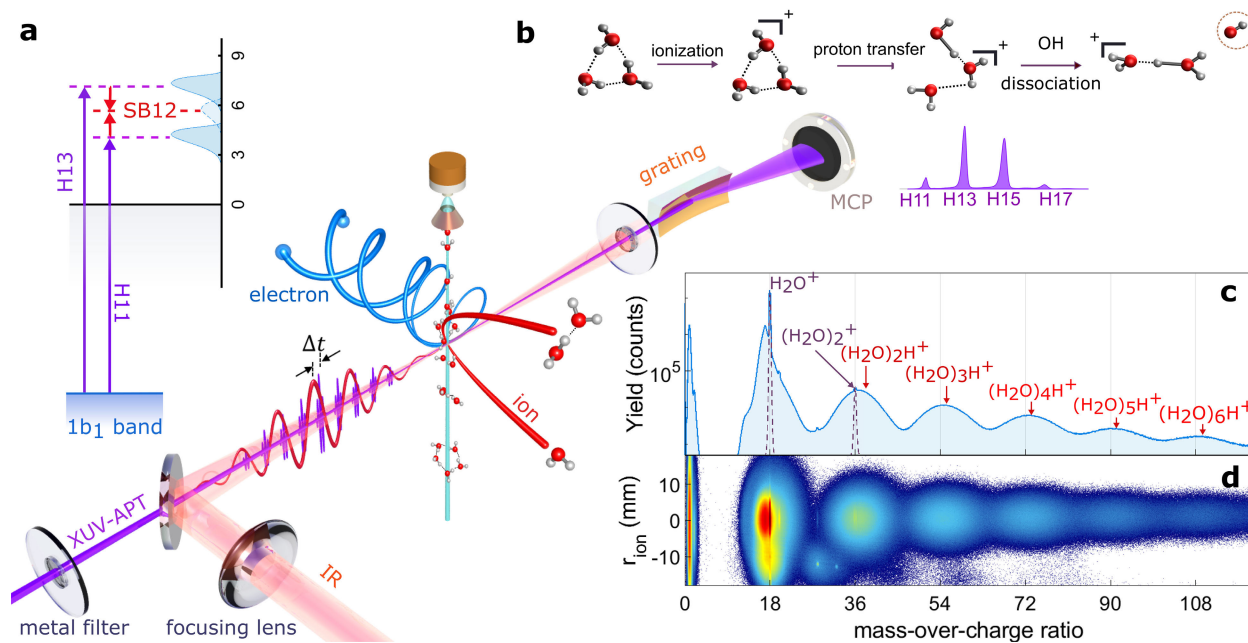
Figure 1: **Attosecond size-resolved cluster spectroscopy. a**, Experimental setup: The charged cluster fragments and emitted photoelectrons are measured in coincidence as a function of the APT-IR delay. The XUV APT is characterized via an online soft-X-ray spectrometer. The inset on the left illustrates ionization by two neighboring harmonic orders and the creation of the sideband spectrum. **b**, Dissociative-ionization mechanism of the water trimer, illustrating the only relevant fragmentation pathway for all observed cluster sizes. **c**, Mass spectrum of the cluster beam photoionized by an APT as a function of the mass-over-charge (MOC) ratio. **d**, Two-dimensional MOC spectrum of water clusters as a function of position on the ion detector.

4

Figure 1 provides a conceptual overview of our measurements. An XUV attosecond pulse train (APT) generated through high-harmonic generation is focused into a supersonic water-cluster beam, where it is spatio-temporally overlapped with a near-infrared (IR) laser pulse. The APT and IR pulses are phase locked through an actively-stabilized Mach-Zehnder interferometer. The three-dimensional momentum distributions of electrons and ions generated from this interaction are detected in coincidence using COLd Target Recoil Ion Momentum Spectroscopy (COLTRIMS)[23–25] [see Methods for details]. The photoionization time delays of water clusters are measured by recording photoelectron spectra as a function of the time delay between the overlapping APT and IR pulses, in coincidence with each ionic fragment. As shown in the inset of Fig. 1a, single-photon XUV ionization gives rise to the main bands (MB) in the photoelectron spectra, whereas the additional IR interaction creates sidebands (SB).

The unique assignment of the coincident attosecond photoelectron spectra to a specific cluster size is possible because of a dissociative-ionization mechanism that is general for small ($< \sim 20$ molecules) water clusters at low ionization energies (Fig. 1b). Following outer-valence single ionization, water clusters undergo rapid proton transfer, followed by the loss of a single OH unit[26–34], such that each detected fragment $(H_2O)_n H^+$ mainly originates from the neutral $(H_2O)_{n+1}$ precursor for n $< 6$ (see SM Section 1.2 for details). The observed mass spectrum (Fig. 1c) indeed shows a well-resolved progression of broad peaks that is easily assigned to $(H_2O)_n H^+$ with $n = 2 - 6$. The width of the peaks is caused by the kinetic-energy release in the dissociative photoionization, as highlighted in Fig. 1d, which shows the mass spectrum as a function of the detected position radius of the ions on the detector ($r_{ion}$). The only unprotonated species ($H_2O^+$ and $(H_2O)_2^+$, purple
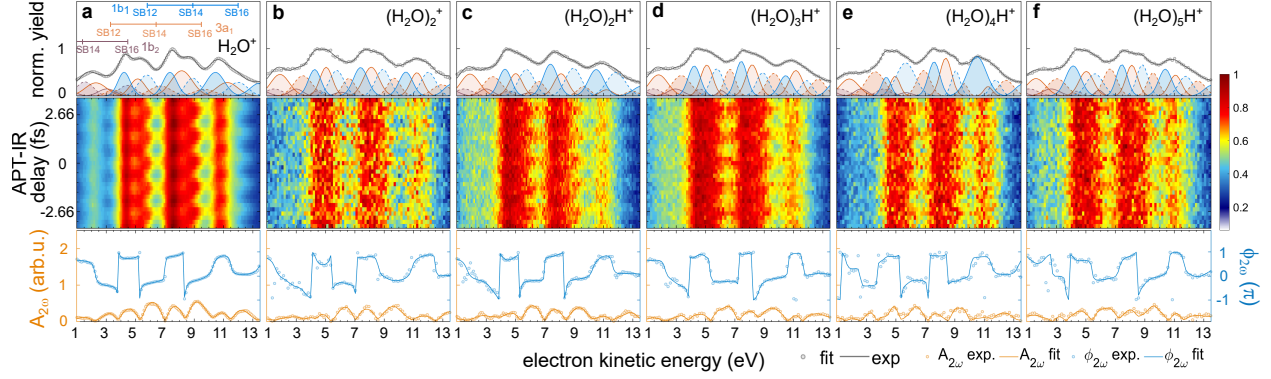
5

Figure 2: **Attosecond photoelectron spectroscopy of size-selected water clusters.** Attosecond photoelectron spectra created by overlapping XUV-APT and IR pulses and detected in coincidence with $H_2O^+$, integrated over the APT-IR delay **a** and shown as a function of APT-IR delay **b**. **c**, Same as **b**, but detected in coincidence with $(H_2O)_2H^+$. The false-color map for **b** and **c** is shown in the top right corner. **d** to **i**, The Fourier transforms at $2\omega$ of the attosecond photoelectron spectra detected in coincidence with **d** $H_2O^+$, **e** $(H_2O)_2^+$, **f** $(H_2O)_2H^+$, **g** $(H_2O)_3H^+$, **h** $(H_2O)_4H^+$, **i** $(H_2O)_5H^+$, shown in terms of their modulation amplitude ($A_{2\omega}$, orange color) and phase ($\phi_{2\omega}$, blue color). The experimental data and the fitted curves are shown as open circles and solid lines, respectively.

dashed curves) originate from the photoionization of $H_2O$ and $(H_2O)_2$, respectively. The broad distribution peaking at a MOC of 17 is $OH^+$ originating from the dissociative ionization of $H_2O^+$. A fraction of the photoionized dimers remains bound, leading to the sharp $(H_2O)_2^+$ peak, and the remainder dissociates to produce $(H_2O)H^+$. Analogous results have been obtained following the ionization of $D_2O$ clusters. The corresponding mass spectra are shown in Fig. S7.

Figure 2 shows the attosecond photoelectron spectra (APS) obtained in coincidence with

each cluster size. The APS measured in coincidence with $H_2O^+$ (Fig. 2a) is dominated by the contributions of harmonic orders 11, 13, and 15, and ionization from the two outermost ($1b_1$ and $3a_1$) molecular orbitals of $H_2O$. The black line shows a fit using the literature values of the vertical binding energies. The filled spectra correspond to the decomposition of the APS in MB (full colored lines) and SB (dashed lines) spectra. Figures 2b and 2c show the characteristic oscillations with a period of 1.33 fs in the APS coincident with $H_2O^+$ and $(H_2O)_2H^+$, respectively. The remaining APS are shown in Fig. S3. Analogous results obtained for $D_2O$ clusters are shown in Fig. S8.

The intensity of SB $q$ oscillates according to $A_q = A_{2\omega,q} \cos(2\omega(\tau - \tau_q^{\mathrm{XUV}} - \tau_q^{\mathrm{sys}})) + B_q$, where $\omega$ is the angular IR frequency, $\tau$ is the experimentally varied APT-IR delay, $\tau_q^{\mathrm{XUV}}$ is the harmonic emission time, and $\tau_q^{\mathrm{sys}}$ is the system-specific photoionization delay measured in sideband $q$. The system-specific photoionization delay can approximately be further decomposed into a continuum-continuum delay $\tau_q^{\mathrm{cc}}$, see Refs.[35,36], induced by the measurement, and a measurement-independent photoionization delay, as discussed in Ref.[37]. Here, we determine relative photoionization delays between water clusters $(H_2O)_n$ and $H_2O$, as a function of $n$, which cancels the contribution of $\tau_q^{\mathrm{XUV}}$. Because the ionization energies vary by less than 0.6 eV from $n = 1 - 6$ [38], the relative measurement also causes negligible contributions of the continuum-continuum (or Coulomb-laser coupling) delays $\tau_q^{\mathrm{cc}}$, on the order of 4-6 as for SB12-14.

The main challenge in the determination of photoionization delays from such measurements is the considerable spectral overlap. We therefore use a general procedure, introduced[39] and vali-

dated in our recent work[6], that resolves this challenge. Instead of integrating the APS oscillations over specific spectral regions, our approach fully accounts for the spectral overlap. Briefly, we Fourier transform the APS along the time-delay axis and then fit the complex-valued Fourier transform at the $2\omega$ frequency by assigning a specific phase shift to each spectral component of the MB and SB spectra. Details are given in the SM, Section 1.5. We keep the spectral positions and amplitudes fixed to values determined from the delay-integrated spectra (see, e.g., Fig. 2a and S3). The success of this fitting procedure is highlighted by the excellent agreement between the experimental data (circles in Figs. 2d-i) and the fits (full lines). The robustness of the fitting procedure to variations of the initial guesses is shown in Fig. S6.

Figures 3a and 3b show the cluster-size-resolved photoionization time delays corresponding to the $1b_1$ photoelectron bands from monomer to hexamer, relative to the monomer delay, as determined from SB12 and SB14, respectively. The time delays measured in SB12 (18.6 eV photon energy) increase as a function of the cluster size up to the tetramer, followed by little variation. The results for SB14 show a similar behavior, with indications of a slightly slower convergence as a function of cluster size. The latter results can be compared to our recent measurements of bulk liquid water[6], which yielded a photoionization delay of 69±20 as relative to the water monomer for SB14, indicated as the red dot in Fig. 3b. The close agreement between the $H_2O$- and $D_2O$- cluster results suggest that nuclear-motion effect are negligible within the accuracy of the present measurements.

To understand the mechanisms governing these delays, we performed *ab-initio* quantum-
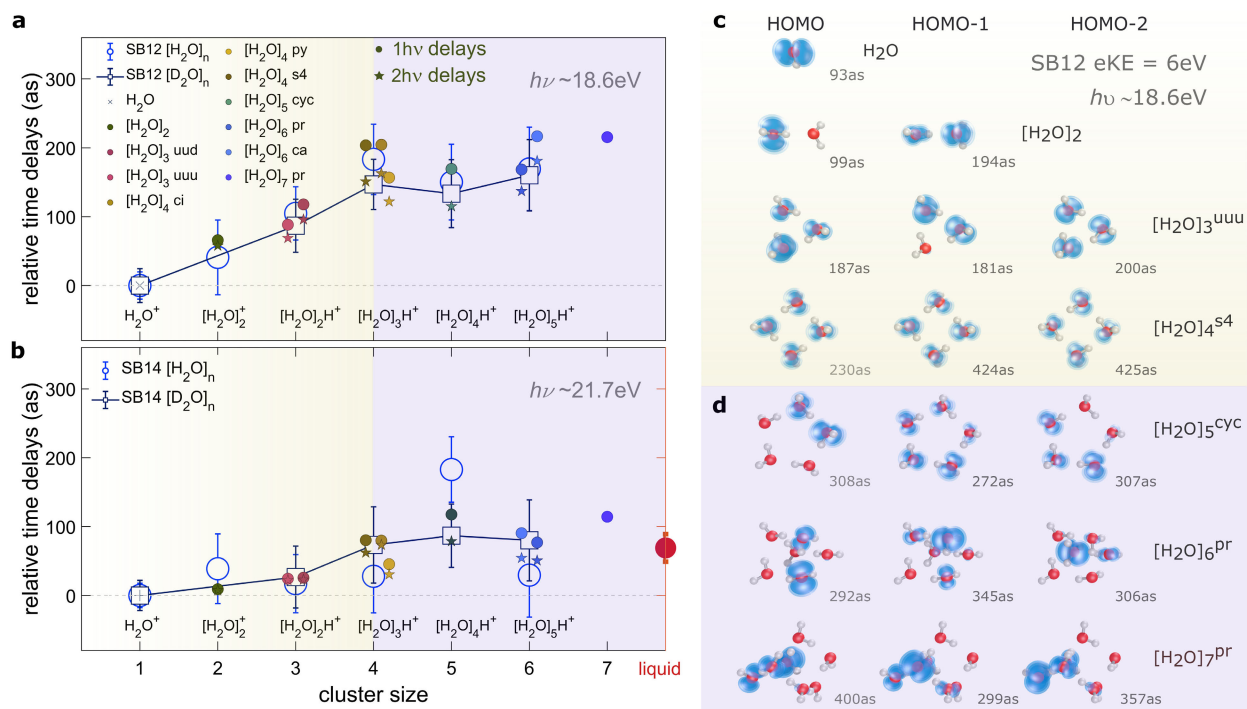
Figure 3: **Size-resolved photoionization time delays of water clusters. a**, Time delays for photoionization out of the $1b_1$ band of water clusters, relative to $H_2O$ (or $D_2O$), measured in SB12 (empty circles). The error bars represent 95% confidence intervals. The calculated delays (filled symbols) were obtained for a kinetic energy of 6.0 eV. **b**, Same as a, but measured for SB14, or calculated with eKE = 9.1 eV, additionally showing the relative photoionization delay of liquid water reported in Ref.[6]. The one-photon (1h$\nu$) and two-photon (2h$\nu$) delay calculations are presented as filled circles and stars, respectively. **c**, Electron density map and calculated absolute photoionization delays of the 1-3 highest-occupied orbitals of the $1b_1$ band of water clusters (designated as "HOMO-$i$"), highlighting the effect of delocalization (yellow shading), followed by partial localization (**d**, violet shading). The structure of the isomers used in the calculation is shown in Table S1 in the supplementary material.

scattering calculations of the photoionization delays (see SM Section 2 and Ref.[37] for details). Starting from the trimer, each water cluster exists in several isomeric forms[40–47]. At the low temperatures reached in our supersonic expansion, only one to three isomers are thermally populated, as detailed in the SM (Section 1.3 and Table S1). We used the equilibrium geometries of the most stable cluster isomers reported in Ref.[41] to perform electronic-structure calculations with a correlation-consistent valence-triple-zeta (cc-pVTZ) basis set. These served as an input to the photoionization calculations performed by solving the electron/water-cluster-ion scattering problem at the experimentally relevant scattering energies using the iterative Schwinger variational principle[48,49]. The input orbitals, scattering potentials and scattering wave functions were all represented by single-center expansions using a typical maximal angular-momentum value of $\ell = 50$, whereby numerical convergence with respect to this parameter was ensured. The photoionization time delays, resolved as a function of photoionization direction in the molecular (cluster) frame and the cluster orientation in the laboratory frame, were obtained and subsequently angularly averaged using the partial photoionization cross sections as weighting factors (for details, see SM Section 2). These calculations yielded angular-integrated one-photon-ionization (or Wigner) delays. We have compared these delays to two-photon (XUV+IR or RABBIT) delays obtained by additionally including the effect of the IR field on the photoionization delays. The results, shown in Figs. S9-S13, establish the close correspondence of angle-resolved one- and two-photon delays in the case of water clusters. Using this methodology, photoionization delays were obtained for each of the $n$ orbitals (HOMO to HOMO-$n$+1) of $(H_2O)_n$ that contribute to the $1b_1$ band of each water cluster. The cross-section-weighted average of these delays (defined in Eq.(1) in the Methods section) are

shown as filled circles (one-photon delays) and filled stars (two-photon delays). The calculated

delays should be understood as containing an error that we estimate to be smaller than 10 as. The

agreement between both types of calculations and the experiment is excellent (Figs. 3a and 3b).

To further challenge the remarkable agreement between experiment and theory, we have per-

formed additional calculations of the photoionization delays with the multi-channel version of the

basis-set complex Kohn variational method[50–52], with details given in the SM (Section 2.6). This

method has the critical advantage of being capable of including the interaction between multiple

photoionization channels, an effect caused by electron correlation. In all of these calculations, all

ion-hole states belonging to the 1b1 band of the water clusters were included and all of the corre-

sponding photoionization channels were coupled, resulting in $n$ coupled channels for $(H_2O)_n$. The

results of these calculations, shown in the Extended Data Figure 1, are again in excellent agree-

ment with the experimental results. This shows that even the inclusion of channel interaction does

not change the agreement between experiment and theory.

Figures 3c and 3d show the densities of the highest-occupied molecular orbitals of the $1b_1$

band of the most stable isomer of each cluster size, together with their absolute one-photon-

ionization delays. All figures in this article are based on Hartree-Fock orbitals, but the corre-

sponding Dyson orbitals only differ in subtle details (see Fig. S24). Figure 3c suggests that the

increasing orbital delocalization correlates with the increasing time delay. The HOMO of the

dimer has almost the same time delay as the monomer, whereas the delocalization of the HOMO-1

in the dimer leads to an increase of the time delay by nearly 100 as. This comparison also shows

the very small effect ($\sim 6$ as) of electron scattering off the neutral $H_2O$ neighbor in the dimer on the photoionization delays of the HOMO. Among the trimer orbitals, it is also the most delocalized orbital (HOMO-2) which has the largest photoionization delay (200 as). The tetramer orbitals are perfectly delocalized over all molecules, owing to the $S_4$ symmetry of its most stable isomer, which leads to the largest photoionization delays (up to 425 as) found in our calculations.

Interestingly, a further increase of the cluster size does not increase the delays further. The reason is obvious from Fig. 3d. Most larger clusters than the tetramer have a lower symmetry, many of them having no symmetry elements at all. This leads to a localization of the orbital densities on a small number of typically 2-3 neighboring molecules. This effect is reflected in a stagnation of the associated photoionization delays around values of $\sim 300$ as in SB12. This observation suggests that the disorder-induced orbital localization in the larger clusters causes the experimentally observed saturation of the measured photoionization delays at the largest cluster sizes measured in this work.

To further verify this surprisingly simple relation between time delays and orbital localization, we performed additional calculations on the oxygen-1s orbitals of the water clusters, with complete results shown in the SM (Figs. S14-S19). The O1s-orbitals have the advantage of remaining essentially atomic in character and not being significantly modified by hydrogen bonding and orbital hybridization. For this reason, they allow us to isolate the effect of orbital (de)localization even more clearly. The results obtained for the O1s-band are shown in Fig. 4b, where they are compared to the results for the $1b_1$ band (Fig. 4a). The photoionization delay remains essentially
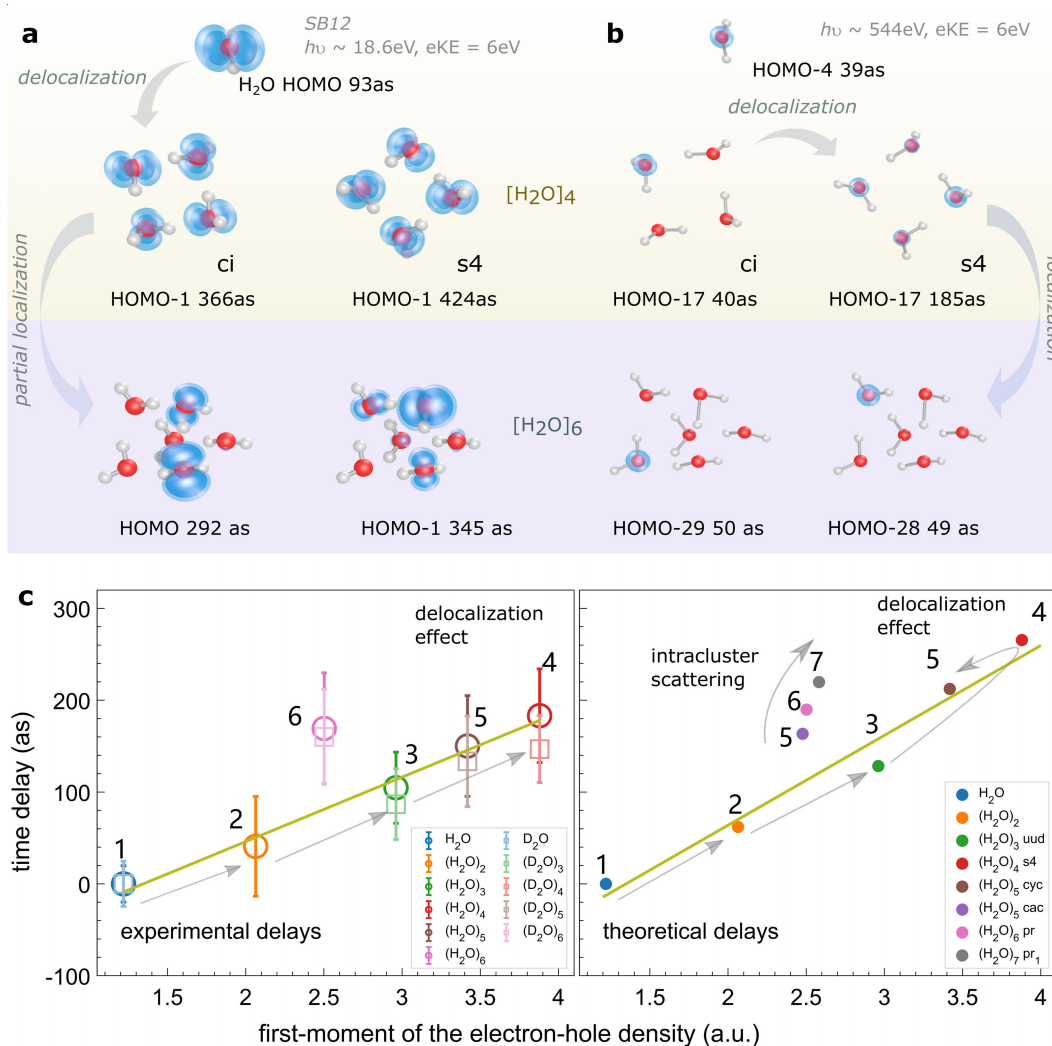
12

Figure 4: **Effect of orbital delocalization on photoionization delays of water clusters a**, Photoionization delays for the $1b_1$ band of water clusters for a kinetic energy of eKE = 6.0 eV, corresponding to the experimental measurements in SB12. **b**, Same as **a**, but for the O1s-band of water clusters using the same kinetic energy, and a correspondingly adjusted photon energy. **c**, Correlation between the photoionization time delays and the first moment of the electron-hole density of the $1b_1$ band of water clusters (eKE = 6.0 eV). The error bars represent 95% confidence intervals.
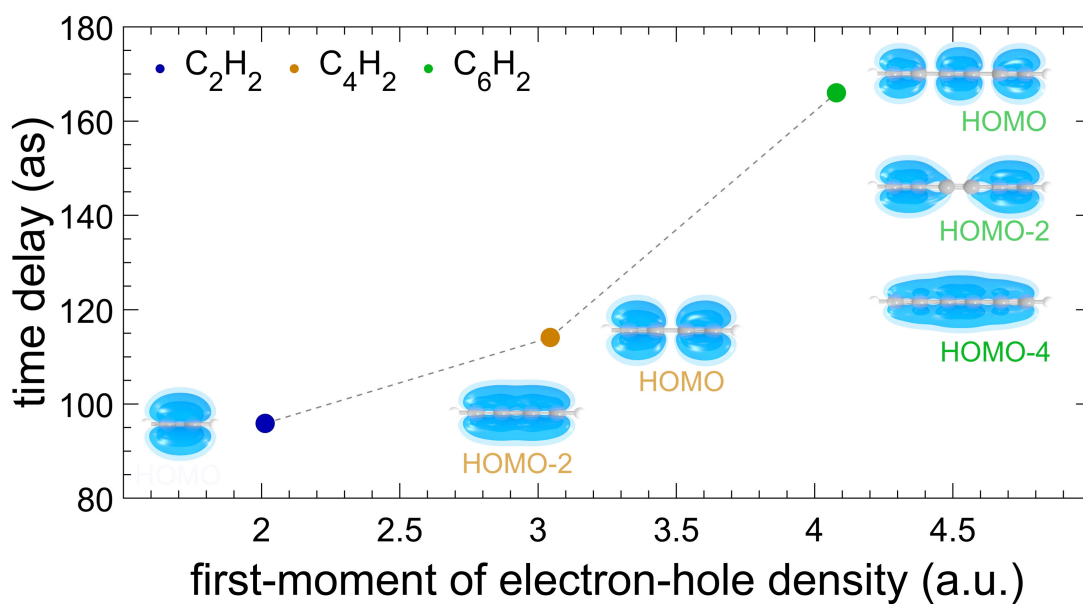
Figure 5: **Effect of orbital delocalization on photoionization delays of poly-acetylenes** Correlation between the photoionization delays and the first moment of the electron-hole density of the $\pi$-orbital-band of acetylene, diacetylene, and triacetylene for a kinetic energy of 6 eV. The insets show the molecular structures and the one-electron density of one of each pair of degenerate contributing orbitals.

unchanged from the monomer (39 as) to the tetramer ci (40 as), where the O-1s orbital is fully

localized, but increases to 185 as in the tetramer s4, where the O-1s orbital is fully delocalized

as a consequence of the high symmetry. Increasing the cluster size further results in a complete

localization of the O-1s orbital, which leads to a remarkable decrease of the photoionization delay

to 49-50 as in the hexamer. The photoionization delays of the O1s orbitals in the hexamer being

practically identical with the monomer (39 as) is again consistent with a direct link between pho-

toionization delays and orbital delocalization. This comparison also confirms the very small effect

(a few attoseconds) of electron scattering off the neutral $H_2O$ moieties contained in the clusters.

The correlation between photoionization delays and electron-hole delocalization also extends to

the $3a_1$ band of water (clusters) as illustrated in the Extended Data Figure 2.

Next, we establish a quantitative correlation between time delays and electron-hole delo-

calization. Figure 4c shows correlation plots between the measured (left) or calculated (right)

photoionization delays of the $1b_1$ band of the water clusters $(H_2O)_n$ and the first moment of the

electron-hole density in the $1b_1$ band of the singly-ionized clusters $(H_2O)_n^+$ (defined in Eqs. (2)-(3)

in Methods). The most stable isomers of all clusters from $n = 1$ to $n = 5$ display a nearly perfect

linear relationship between the two quantities, as indicated by the straight lines in Fig. 4c. This

representation also highlights the continuous increase of the delocalization from $n = 1$ to $n = 4$,

followed by partial localization at $n = 5 - 7$, visible in the fact that the second-most stable isomer

of $n = 5$ and the most stable isomers of $n = 6$ and 7 have nearly the same first moment of the

electron-hole density. Interestingly, the delays of the latter three isomers display a continuous,

yet very small increase, which we assign to intracluster scattering, quantifying this effect as well.

15

The robustness of the electron-hole delocalization to thermal excitation in our experiments has been verified by running ab-initio molecular-dynamics (AIMD) simulations, as illustrated in the Extended Data Figure 3.

These results have a range of interesting implications. First, they demonstrate the existence of a correlation between photoionization delays and orbital delocalization in water clusters, which, to our knowledge, could not be experimentally quantified in any form of matter so far. Second, they reveal the mechanism that is responsible for orbital localization in liquid water on the molecular level, i.e. the onset of structural disorder. This effect is reminiscent of Anderson localization in solids[16]. Whereas perfect crystals with translational symmetry have fully delocalized bands, the presence of defects causes their localization, which has a multitude of interesting consequences in solid-state physics. Similarly, the high point-group symmetry of small water clusters is broken at the transition to bulk liquid water, which results in a partial localization of the electronic wave functions in liquid water, offering an intuitive interpretation of our present and previous[6] results.

Finally, we study the extension of our results to other systems. A particularly attractive class are the polyacetylene systems because of their use in molecular electronics and conductive polymers[53]. Figure 5 shows that the photoionization delays in this class of systems also display a quasi-linear correlation with the first moment of the associated electron-hole density. This finding suggests the possibility of experimentally measuring the degree of electron/hole-delocalization in acetylene-based polymers and, in future pump-probe experiments, to follow charge transport in such systems on the electronic time scale.

Before concluding, we note that the discussed correlations do not imply that electron-hole delocalization is the only possible explanation of the observed time-delay effects. Instead, the delays could also reflect a more fundamental property, of which the orbital delocalization is one consequence. One such property could e.g. be the ratio between the electronic interaction matrix elements between the subunits (e.g. water monomers) and the difference in the electronic binding energies of the non-interacting subunits. When this ratio is large, electrons can easily move from one subunit to another, leading to strong orbital delocalization. When this ratio is small, the electron mobility is suppressed, which is also the case in liquids and amorphous solids. The outlined correlations could thus also be interpreted as reflecting electron mobility in matter on a purely electronic time scale, a specification imposed by the attosecond time scale of photoemission.

We have introduced a new technique, ASCS, and have applied it to measure photoionization time delays of size-resolved water clusters. This study has revealed an unexpectedly simple relationship between orbital localization and time delays, establishing an experimental pathway to probing electron-hole localization in complex matter. Looking forward, our methods can be used to temporally resolve both local and non-local electronic relaxation dynamics in size-resolved water clusters, such as Auger decay, intermolecular Coulombic decay[54,55] and electron-transfer-mediated decay[56]. More generally, they will facilitate a molecular-level understanding of attosecond electron dynamics in the liquid phase, with implications for the elementary processes underlying chemical reactivity and biological function.

17

**Methods**

**Laser Setup and Attosecond-Pulse Generation** The experimental setup is based on a regeneratively amplified Titanium-Sapphire laser system which delivers near-infrared (IR) femtosecond laser pulses at 5 kHz repetition rate, a central wavelength of 800 nm, a bandwidth of 40 nm, and 36 fs pulse duration (full-width at half-maximum in intensity). This laser beam is split with a 70:30 beam splitter and the more intense part (0.4 mJ, with a beam diameter of 10 mm) is focused (f=40 cm) into a 3 mm long, xenon-filled gas cell to generate an extreme-ultraviolet attosecond pulse train (XUV-APT) via high-harmonic generation. A coaxial 100-nm aluminum foil on a quartz ring is placed before a nickel-coated toroidal mirror ($f = 50$ cm) to spectrally filter the XUV spectrum and eliminate the residual IR pulse co-propagating with the XUV beam. The XUV spectrum was characterized with a home-built XUV spectrometer consisting of a 100-nm aluminum film, an aberration-corrected flat-field grating (Shimadzu 1200 lines/mm) and a micro-channel-plate (MCP) detector coupled to a phosphor screen. The XUV flux was estimated to be on the order of $10^7$ photons per shot.

The XUV-APT is recombined with the remaining part of the IR beam after the toroidal mirror via a perforated silver mirror to constitute a Mach-Zehnder interferometer. The path length difference, i.e. the time delay between the overlapping XUV-APT and IR pulses is controlled via a high-precision direct-current motor (PI, resolution 0.1 $\mu$m) and a piezoelectric motor (PI, resolution 0.1 nm), constituting a combined delay stage operating on femtosecond and attosecond time scales, respectively. The pulse energy of the dressing IR field was 0.08 mJ before the perforated mirror, focused with f=1.0 m. The focal spot size of the dressing IR field as measured by a camera

18

was 120 $\mu$m and that of the XUV was estimated to be around 50 $\mu$m. The peak intensity of the dressing IR field was estimated to be below 1 TW/cm$^2$.

**Coincidence Spectrometer** The phase-locked XUV-APT and IR pulses are collinearly focused into the supersonic gas jet in a COLTRIMS (COLd Target Recoil Ion Momentum Spectroscopy)[23–25] spectrometer. The electrons and ions created by XUV photoionization are guided by a weak homogeneous electric field (3.20 V·cm$^{-1}$) and a homogeneous magnetic field (6.70 G) towards two time- and position-sensitive detectors at opposite ends of the spectrometer. The detectors consist of two MCPs (Photonis) in Chevron configuration, followed by a three-layer delay-line anode (HEX) with a crossing angle of 60 degrees between adjacent layers and an active radius of 40 mm manufactured by RoentDek. For the electrons, the length of the extraction region is 7 cm, followed by a 14 cm field-free region. A homogeneous magnetic field is applied over all regions by a set of Helmholtz coils, which are tilted to counteract the earth's magnetic field. The COLTRIMS gives access to the typical electron-ion coincidence measurement with full three-dimensional momentum resolution in 4$\pi$ solid angle. The momentum resolution of electrons is $\Delta p_x = \Delta p_y = 0.001$ a.u. and $\Delta p_z = 0.0056$ a.u., where $x$ corresponds to the direction of light propagation, $y$ is the direction of the supersonic gas jet and $z$ is the time-of-flight direction. The photoelectron kinetic energy is calibrated via the XUV-APT photoelectron spectrum of argon with an ionization potential of $I_p \sim$ 15.8 eV.

**Cluster source** The neutral water clusters[57,58] are formed in a continuous supersonic expansion into vacuum with a water vapor pressure of 0.3 MPa through a 50 $\mu$m nozzle orifice and pass through two conical skimmers (Beam Dynamics) located 10 mm and 30 mm downstream with a

diameter of 200 $\mu$m and 1 mm, respectively. The liquid water is maintained at 408 K to give rise to a sufficient vapor pressure in a container of 0.7 L to support a stable water-cluster beam for a duration of 120 hours. The water-cluster source is coupled to the COLTRIMS via two differential pumping stages. To maintain the ultrahigh vacuum in the main reaction chamber, a differentially pumped beam dump captures the molecular beam after the interaction region. The internal temperature of the clusters in the beam is estimated to be around 100 K (see SM for details).

**Definition of the calculated quantities** The calculation of the orbital-specific photoionization delays is described in the main text and in more detail in Section 2 of the SM. Here, we additionally define the cross-section-averaged delays shown in Figs. 3a, 3b as large empty circles and also in Fig. 4c. Since the contributions of individual orbitals to the $1b_1$ band of the water clusters cannot be resolved, we introduce the cross-section-average of the time delays over the $n$ orbitals constituting the $1b_1$ band of $(H_2O)_n$ as follows:

$$\tau(E) = \frac{\sum_{i=1}^{n} \sigma_i(E)\tau_i(E)}{\sum_{i=1}^{n} \sigma_i(E)}, \tag{1}$$

where $\sigma_i(E)$ is the photoionization cross section of orbital $i$ of the $1b_1$ band at the photon energy $E$ and $\tau_i(E)$ is the corresponding photoionization time delay.

In Fig. 4c, we additionally show the first moment of the electron-hole density, calculated using ORBKIT package[59]. In the case of a single orbital (with index $i$) this is defined as

$$\mathcal{M}_i = \frac{\int \rho_i(\vec{r} - \vec{r_i}) \, |\vec{r} - \vec{r_i}| \, d^3r}{\int \rho_i(\vec{r}) d^3r}, \tag{2}$$

where $\rho_i(\vec{r})$ is the density of orbital $i$ and $\vec{r_i}$ is its center of charge. In analogy to the time delays,

we also define a cross-section average of the orbital delocalization as

$$\mathcal{M} = \frac{\sum_{i=1}^{n} \sigma_i \mathcal{M}_i}{\sum_{i=1}^{n} \sigma_i}, \tag{3}$$
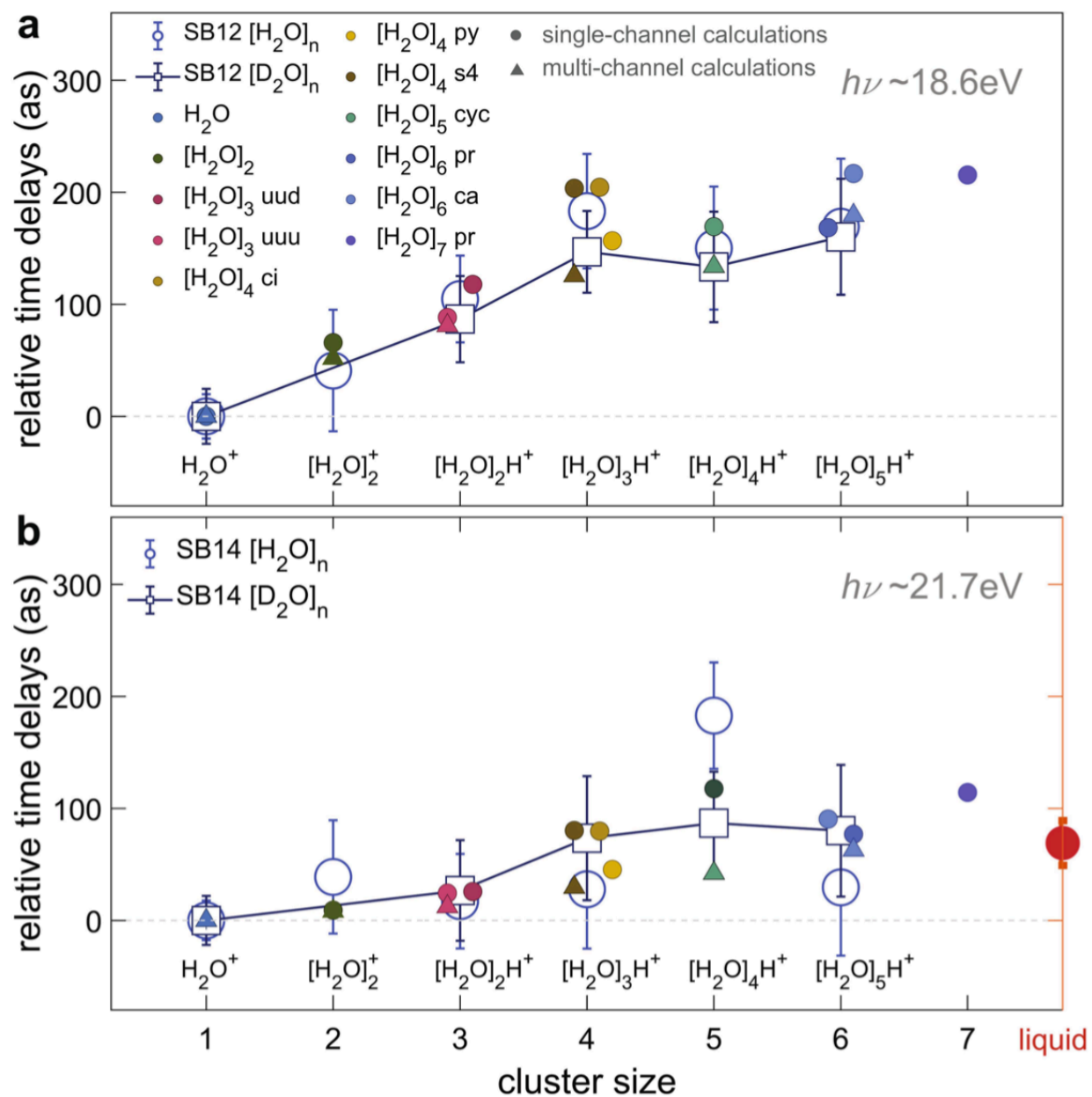
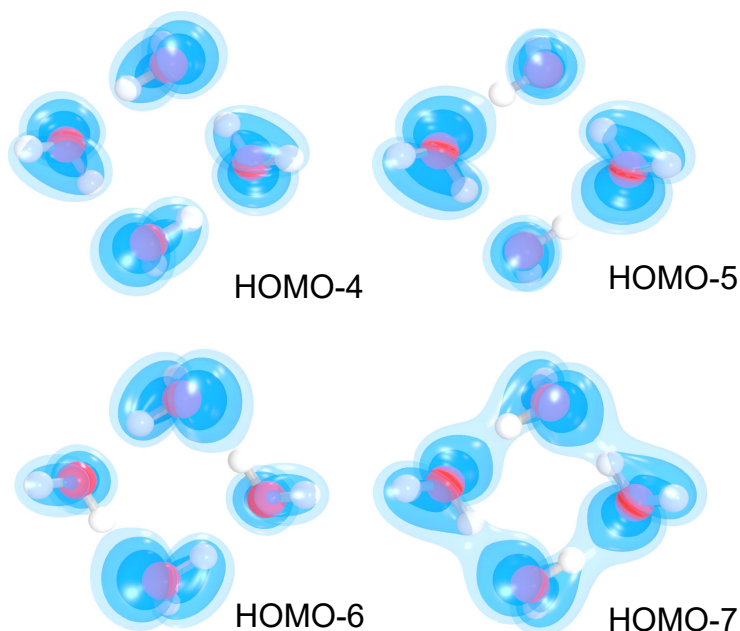**Extended Data Figure 1: Effect of the channel coupling on photoionization delays of the 1b$_1$ band. a**, Calculated time delays for photoionization out of the 1b$_1$ band of water clusters relative to H$_2$O for a kinetic energy of eKE = 6.0 eV (SB12). The results of the single-channel calculations using ePolyScat[48,49] (filled circles) are compared with multi-channel calculations using the basis-set complex Kohn method[50–52] (filled triangles) are compared. The experimental results are identical to those shown in Fig. 3. **b**, Same as **a**, but calculated/measured for SB14.

H$_2$O
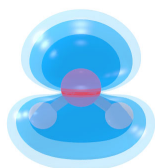
HOMO-1
deloc. mom. = 1.4 a.u.
delay = 96 as

(H$_2$O)$_4$ S4

HOMO-4

HOMO-5

HOMO-6

HOMO-7

deloc. mom. = 3.96 a.u.
delay = 243 as

**Extended Data Figure 2: Effect of orbital delocalization on photoionization delays of the 3a$_1$ band.** Correlation between the photoionization delays and the first moment of the electron-hole density of the 3a$_1$-orbital-band of water monomer and tetramer (S4) for a kinetic energy of eKE = 6 eV.
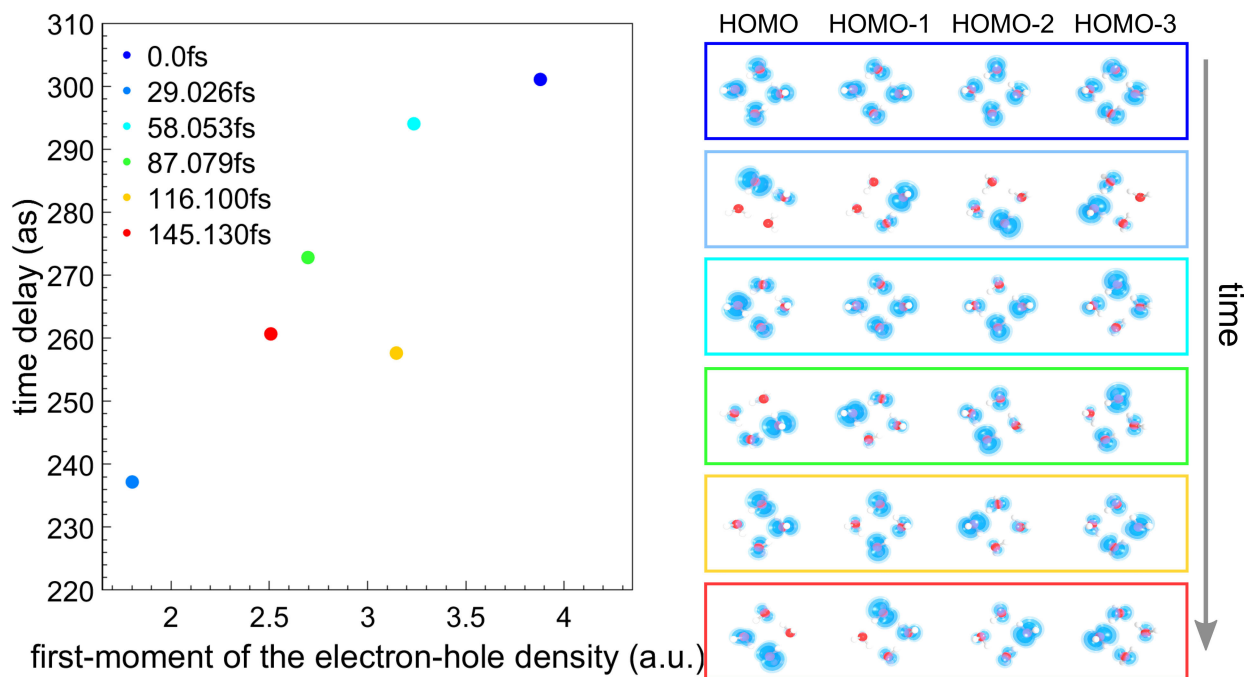
**Extended Data Figure 3: Effect of molecular geometry on orbital delocalization and pho-toionization delays of (H$_2$O)$_4$ S4.** The structures are obtained from AIMD time propagation for different times (see legend). AIMD are run using density-functional theory, the Turbomole software package, B3-LYP density functional, def2-TZVP basis and a temperature of T=100 K.

# References

1. Sanche, L. Beyond radical thinking. *Nature* **461**, 358–359 (2009).

2. Boudaiffa, B., Cloutier, P., Hunting, D., Huels, M. A. & Sanche, L. Resonant formation of dna strand breaks by low-energy (3 to 20 ev) electrons. *Science* **287**, 1658–1660 (2000). URL `http://www.sciencemag.org/content/287/5458/1658.abstract`.

3. Garrett, B. C. *et al.* Role of water in electron-initiated processes and radical chemistry: Issues and scientific advances. *Chemical reviews* **105**, 355–390 (2005).

4. Svoboda, V. *et al.* Real-time observation of water radiolysis and hydrated electron formation induced by extreme-ultraviolet pulses. *Science Advances* **6**, eaaz0385 (2020).

5. Loh, Z.-H. *et al.* Observation of the fastest chemical processes in the radiolysis of water. *Science* **367**, 179–182 (2020).

6. Jordan, I. *et al.* Attosecond spectroscopy of liquid water. *Science* **369**, 974–979 (2020). URL `https://doi.org/10.1126/science.abb0979`.

7. Cavalieri, A. L. *et al.* Attosecond spectroscopy in condensed matter. *Nature* **449**, 1029 (2007). URL `http://dx.doi.org/10.1038/nature06229`.

8. Schultze, M. *et al.* Delay in photoemission. *Science* **328**, 1658–1662 (2010). URL `http://www.sciencemag.org/cgi/content/abstract/328/5986/1658`.

9. Klünder, K. *et al.* Probing single-photon ionization on the attosecond time scale. *Phys. Rev. Lett.* **106**, 143002 (2011). URL http://link.aps.org/doi/10.1103/PhysRevLett.106.143002.

10. Ossiander, M. *et al.* Attosecond correlation dynamics. *Nature Physics* **13**, 280–285 (2016).

11. Huppert, M., Jordan, I., Baykusheva, D., von Conta, A. & Wörner, H. J. Attosecond delays in molecular photoionization. *Phys. Rev. Lett.* **117** (2016).

12. Alizadeh, E., Orlando, T. M. & Sanche, L. Biomolecular damage induced by ionizing radiation: the direct and indirect effects of low-energy electrons on dna. *Annual review of physical chemistry* **66**, 379–398 (2015).

13. Marsalek, O. *et al.* Chasing charge localization and chemical reactivity following photoionization in liquid water. *The Journal of chemical physics* **135**, 224510 (2011).

14. Cattaneo, L. *et al.* Attosecond coupled electron and nuclear dynamics in dissociative ionization of $H_2$. *Nature Physics* **14**, 733–739 (2018).

15. Nandi, S. *et al.* Attosecond timing of electron emission from a molecular shape resonance. *Science Advances* **6**, eaba7762 (2020).

16. Anderson, P. W. Absence of diffusion in certain random lattices. *Physical Review* **109**, 1492–1505 (1958). URL https://doi.org/10.1103/PhysRev.109.1492.

17. Anderson, P. W. *Basic notions of condensed matter physics* (Westview Press, 1997). URL https://doi.org/10.4324/9780429494116.

18. Hunt, P., Sprik, M. & Vuilleumier, R. Thermal versus electronic broadening in the density of states of liquid water. *Chemical physics letters* **376**, 68–74 (2003).

19. Prendergast, D., Grossman, J. C. & Galli, G. The electronic structure of liquid water within density-functional theory. *The Journal of chemical physics* **123**, 014501 (2005).

20. Pieniazek, P. A., Sundstrom, E. J., Bradforth, S. E. & Krylov, A. I. Degree of initial hole localization/delocalization in ionized water clusters. *The Journal of Physical Chemistry A* **113**, 4423–4429 (2009).

21. Winter, B. *et al.* Full valence band photoemission from liquid water using euv synchrotron radiation. *J. Phys. Chem. A* **108**, 2625–2632 (2004). URL `http://dx.doi.org/10.1021/jp030263q`.

22. Pohl, M. N. *et al.* Do water's electrons care about electrolytes? *Chemical science* **10**, 848–865 (2019).

23. Dörner, R. *et al.* Cold Target Recoil Ion Momentum Spectroscopy: A 'momentum microscope' to view atomic collision dynamics. *Physics Report* **330**, 95–192 (2000). URL `https://doi.org/10.1016/S0370-1573(99)00109-X`.

24. Jagutzki, O. *et al.* Multiple hit readout of a microchannel plate detector with a three-layer delay-line anode. *IEEE Transactions on Nuclear Science* **49 II**, 2477–2483 (2002). URL `https://doi.org/10.1109/TNS.2002.803889`.

25. Ullrich, J. *et al.*  Recoil-ion and electron momentum spectroscopy:  reaction-microscopes.  *Reports on Progress in Physics* **66**, 1463–1545 (2003).  URL https://doi.org/10.1088/0034-4885/66/9/203.

26. Dong, F., Heinbuch, S., Rocca, J. J. & Bernstein, E. R.  Dynamics and fragmentation of van der Waals clusters: (H 2O) n, (CH 3OH) n, and (NH 3) n upon ionization by a 26.5 eV soft x-ray laser. *Journal of Chemical Physics* **124**, 224319 (2006).

27. Shiromaru, H., Shinohara, H., Washida, N., Yoo, H. & Kimura, K.  Synchrotron radiation measurements of appearance potentials for (H2O)2+, (H2O)3+,(H2O)2H+ and (H2O)3H+ in supersonic jets. *Chemical physics letters* **141**, 7–11 (1987).

28. Shi, Z., Ford, J. V., Wei, S. & Castleman, A. W.  Water clusters: Contributions of binding energy and entropy to stability. *The Journal of Chemical Physics* **99**, 8009–8015 (1993).

29. Wei, S. & Castleman, A. W.  Using reflection time-of-flight mass spectrometer techniques to investigate cluster dynamics and bonding. *International Journal of Mass Spectrometry and Ion Processes* **131**, 233–264 (1994).

30. Bobbert, C., Schütte, S., Steinbach, C. & Buck, U.  Fragmentation and reliable size distributions of large ammonia and water clusters. *The European Physical Journal D* **19**, 183–192 (2002). URL https://doi.org/10.1140/epjd/e20020070.

31. Tachikawa, H.  Ionization Dynamics of the Small-Sized Water Clusters: A Direct Ab Initio Trajectory Study. *The Journal of Physical Chemistry A* **108**, 7853–7862 (2004).  URL https://doi.org/10.1021/jp049269l.

32. Belau, L., Wilson, K. R., Leone, S. R. & Ahmed, M. Vacuum ultraviolet (VUV) photoionization of small water clusters. *Journal of Physical Chemistry A* **111**, 10075–10083 (2007). URL `https://doi.org/10.1021/jp075263v`.

33. Liu, X., Lu, W. C., Wang, C. Z. & Ho, K. M. Energetic and fragmentation stability of water clusters $(H_2O)_n$, n = 2-30. *Chemical Physics Letters* **508**, 270–275 (2011). URL `https://doi.org/10.1016/j.cplett.2011.04.055`.

34. Zamith, S., Labastie, P. & Lhermite, J. M. Fragmentation cross sections of protonated water clusters. *Journal of Chemical Physics* **136**, 214301 (2012). URL `https://doi.org/10.1063/1.4722886`.

35. Dahlström, J. M., L'Huillier, A. & Maquet, A. Introduction to attosecond delays in photoionization. *Journal of Physics B: Atomic, Molecular and Optical Physics* **45**, 183001 (2012). URL `http://stacks.iop.org/0953-4075/45/i=18/a=183001`.

36. Pazourek, R., Nagele, S. & Burgdörfer, J. Attosecond chronoscopy of photoemission. *Rev. Mod. Phys.* **87**, 765–802 (2015). URL `http://link.aps.org/doi/10.1103/RevModPhys.87.765`.

37. Baykusheva, D. & Wörner, H. J. Theory of attosecond delays in molecular photoionization. *The Journal of Chemical Physics* **146**, 124306 (2017). URL `http://dx.doi.org/10.1063/1.4977933`.

38. Barth, S. *et al.* Valence ionization of water clusters: From isolated molecules to bulk. *Journal of Physical Chemistry A* **113**, 13519–13527 (2009). URL https://doi.org/10.1021/jp906113e.

39. Jordan, I., Jain, A., Gaumnitz, T., Ma, J. & Wörner, H. J. Photoelectron spectrometer for liquid and gas-phase attosecond spectroscopy with field-free and magnetic bottle operation modes. *Review of Scientific Instruments* **89**, 053103 (2018). URL https://doi.org/10.1063/1.5011657.

40. Shi, Z., Ford, J. V., Wei, S. & Castleman, A. W. Water clusters: Contributions of binding energy and entropy to stability. *The Journal of Chemical Physics* **99**, 8009–8015 (1993). URL https://doi.org/10.1063/1.465678.

41. Temelso, B., Archer, K. A. & Shields, G. C. Benchmark structures and binding energies of small water clusters with anharmonicity corrections. *Journal of Physical Chemistry A* **115**, 12034–12046 (2011). URL https://doi.org/10.1021/jp2069489.

42. Malloum, A., Fifen, J. J., Dhaouadi, Z., Nana Engo, S. G. & Conradie, J. Structures, relative stability and binding energies of neutral water clusters,$H_2O_n$, $n$ = 2-30. *New Journal of Chemistry* **43**, 13020–13037 (2019). URL https://doi.org/10.1039/c9nj01659g.

43. Liu, K. *et al.* Characterization of a cage form of the water hexamer. *Nature* **381**, 501–503 (1996). URL https://doi.org/10.1038/381501a0.

44. Liu, K., Cruzan, J. D. & Saykally, R. J. Water clusters. *Science* **271**, 929–933 (1996). URL https://doi.org/10.1126/science.271.5251.929.

45. Xantheas, S. S. Cooperativity and hydrogen bonding network in water clusters. *Chemical Physics* **258**, 225–231 (2000). URL https://doi.org/10.1016/S0301-0104(00)00189-0.

46. Richardson, J. O. *et al.* Concerted hydrogen-bond breaking by quantum tunneling in the water hexamer prism. *Science* **351**, 1310–1313 (2016). URL https://doi.org/10.1126/science.aae0012.

47. Cvitaš, M. T. & Richardson, J. O. Quantum tunnelling pathways of the water pentamer. *Physical Chemistry Chemical Physics* **22**, 1035–1044 (2020). URL https://doi.org/10.1039/c9cp05561d.

48. Gianturco, F. A., Lucchese, R. R. & Sanna, N. Calculation of low-energy elastic cross sections for electron-cf4 scattering. *Journal of Chemical Physics* **100**, 6464–6471 (1994).

49. Natalense, A. P. P. & Lucchese, R. R. Cross section and asymmetry parameter calculation for sulfur 1s photoionization of sf6. *Journal of Chemical Physics* **111**, 5344–5348 (1999).

50. Rescigno, T. N., Lengsfield III, B. H. & McCurdy, C. W. The incorporation of modern electronic structure methods in electron-molecule collision problems: Varaiational calculations using the complex kohn method. In Yarkony, D. R. (ed.) *Modern Electronic Structure Theory*, vol. 1, 501–588 (World Scientific, Singapore, 1995).

51. Rescigno, T. N., McCurdy, C. W., Orel, A. E. & Lengsfield III, B. H. The complex kohn variational method. In *Computational Methods for Electron-Molecule Collisions*, 1–44 (Springer, 1995).

52. Orel, A. E. & Rescigno, T. N. Variational expressions for first-order properties involving continuum wave functions. *Phys. Rev. A* **41**, 1695–1697 (1990).

53. Silvestri, F. & Marrocchi, A. Acetylene-based materials in organic photovoltaics. *International journal of molecular sciences* **11**, 1471–1508 (2010).

54. Jahnke, T. *et al.* Ultrafast energy transfer between water molecules. *Nature Physics* **6**, 139–142 (2010). URL http://dx.doi.org/10.1038/nphys1498.

55. Mucke, M. *et al.* A hitherto unrecognized source of low-energy electrons in water. *Nature Physics* **6**, 143–146 (2010). URL http://dx.doi.org/10.1038/nphys1500.

56. Unger, I. *et al.* Observation of electron-transfer-mediated decay in aqueous solution. *Nature Chemistry* **9**, 708 (2017).

57. Hagena, O. F. & Obert, W. Cluster formation in expanding supersonic jets: effect of pressure, temperature, nozzle size, and test gas. *The Journal of Chemical Physics* **56**, 1793–1802 (1972). URL https://doi.org/10.1063/1.1677455.

58. Pradzynski, C. C., Forck, R. M., Zeuch, T., Slavíček, P. & Buck, U. A fully size-resolved perspective on the crystallization of water clusters. *Science* **337**, 1529–1532 (2012). URL https://doi.org/10.1126/science.1225468.

59. Hermann, G. *et al.* Orbkit: A modular python toolbox for cross-platform postprocessing of quantum chemical wavefunction data. *Journal of Computational Chemistry* **37**, 1511–1520 (2016).

**Author contributions**    X.G. and S.H. carried out the experiments and analysed the experimental data. X.G. constructed the experimental apparatus with contributions from S.H., K.Z. and C.P.. D.J. performed the majority of the theoretical calculations. R.L. realized the basis-set complet Kohn variational calculations. X.G., S.H., and H.J.W wrote the initial manuscript. All authors discussed and reviewed the manuscript.

**Competing Interests**    The authors declare no competing interests.

**Supplementary information**    is available for this paper.

**Correspondence and requests for materials**    should be addressed to H.J.W.

**Data availability statement**    All data is available from the corresponding author on request.